Appendix for:

Recent advances in the diagnosis and prognosis of ALS

Stephen A Goutman,[1] MD, Orla Hardiman,[2] MD, Ammar Al-Chalabi,[3] PhD, FRCP, Dip.Stat, Adriano Chió,[4] MD, Masha G Savelieff,[1] PhD, Matthew C. Kiernan,[5] AM, PhD, DSc, Eva L Feldman,[1] MD, PhD

[1]University of Michigan, Ann Arbor, MI, United States

[2]Trinity College Dublin, Dublin, Ireland

[3]King's College London, London, United Kingdom

[4]'Rita Levi Montalcini' Department of Neurosciences, University of Turin, Piemonte, Italy

[5]Brain and Mind Centre, University of Sydney; and Department of Neurology, Royal Prince Alfred Hospital, Sydney, Australia

Authors		
Stephen A Goutman	sgoutman@med.umich.edu	0000-0001-8780-6637
Orla Hardiman	orla@hardiman.net	0000-0003-2610-1291
Ammar Al-Chalabi	ammar.al-chalabi@kcl.ac.uk	0000-0002-4924-7712
Adriano Chió	adriano.chio@unito.it	0000-0001-9579-5341
Masha G Savelieff	savelief@umich.edu	0000-0001-5575-2494
Matthew C Kiernan	matthew.kiernan@sydney.edu.au	0000-0001-9054-026X
Eva L Feldman	efeldman@umich.edu	0000-0002-9162-2694

Correspondence to:

Eva L Feldman MD, PhD

efeldman@umich.edu

Department of Neurology

Michigan Medicine

University of Michigan

Ann Arbor, MI 48109

United States

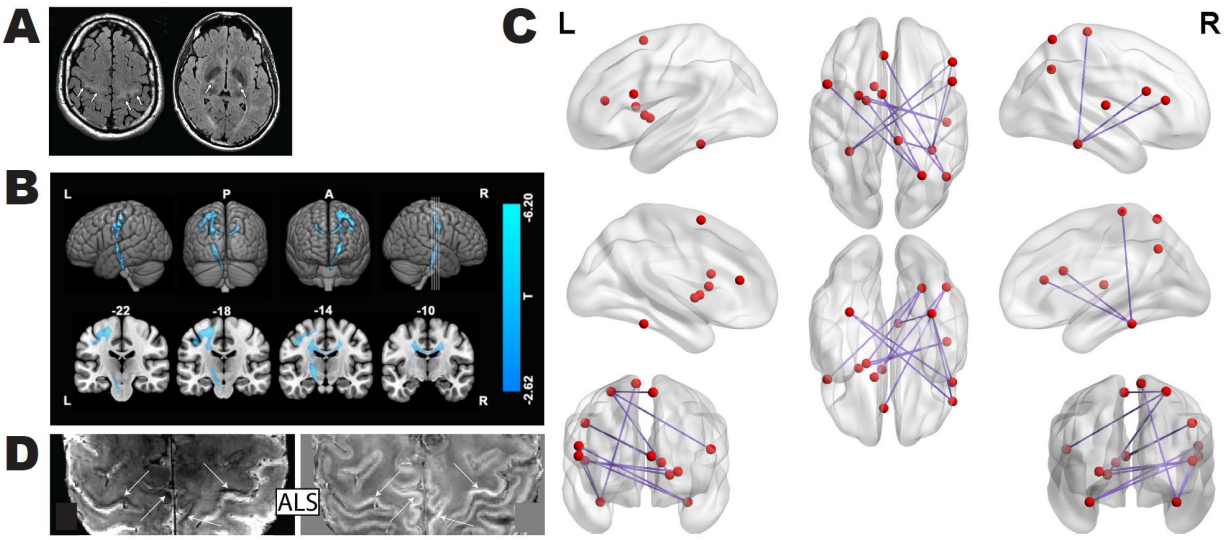

Figure 1. Brain imaging in ALS. (**A**) Routine MRI FLAIR (fluid-attenuated inversion recovery) of ALS brain. Arrows represent bilateral hyperintensities in the corticospinal tract (CST). (**B**) Diffusion tensor imaging (DTI) of white matter changes in ALS patients. Top panel: 3D rendered white matter tracts with lower fractional anisotropy in ALS versus HC. Bottom panel: Four coronal slices of white matter tracts with lower fractional anisotropy in ALS versus HC. Color scale: Represents t values. Results adjusted for multiple comparisons by Gaussian random field theory. A, anterior; L, left; P, posterior; R, right. (**C**) Connectome mapping by network-based analysis of resting-state global connectivity. Edges represent higher connectivity ($p<0{\cdot}05$); in ALS this involves certain frontal, parietal, subcortical, and temporal regions, represented by red nodes. L, left; R, right. (**D**) Quantitative susceptibility mapping (QSM), surrogate of iron deposition, of primary motor cortex in ALS. Left panel: T2*-weighted images of primary motor cortex. Right panel: Corresponding QSM map of primary motor cortex. Arrows represent T2* signal hypointensity and QSM hyperintensity in ALS primary motor cortex deep layers. Adapted with permissions from (A) Mazón et al. Front Neurosci 2018,[1] (B) Qiu et al. Hum Brain Mapp 2019,[2] (C) Geevasinga et al. Eur J Neurol 2017,[3] and (D) Costagli et al. NeuroiImage: Clinical 2016.[4]

Table. Brain Imaging studies. Case/control brain-based imaging studies of human ALS participants in the last five years, meeting the criteria English language article with ALS > 20 participants. Studies listed in alphabetical order by first author name.

Reference	Modality	Population	Findings in ALS participants
"MRI" search criterion			
Acosta-Cabronero[5]	QSM, MRI	28 ALS 39 controls	Higher QSM in ALS motor cortex, left substantial nigra, globus pallidus, red nucleus; lower QSM in CST white matter.
Alruwaili[6]	T1, DWI	30 ALS 19 controls	Lower FA in CST, callosal radiation and body of corpus callosum, cingulum, superior/inferior longitudinal fasciculus; higher MD in CST, cingulum, anterior thalamic radiation, corpus callosum, inferior longitudinal fasciculus, uncinated fasciculus; findings more pronounced in ALS patients with vs without cognitive involvement.
Baek[7]	DTI	96 ALS 47 controls	Decreased FA in corpus callosum, bilateral CST, bilateral cerebral and cerebellar peduncles; decreased AD in bilateral CST; increased AD in corpus callosum and and bilateral corona radiata; increased RD and MD in corpus callosum and bilateral corona radiata; increased in bilateral cerebral peduncles and left cerebellar peduncle. Decreased MO in corpus callosum and left CST; increased MO in bilateral internal capsule; multiple DTI parameters and regions correlated with ALSFRS-R and change in ALSFRS-R; DTI parameters did not distinguish ALS groups by rate of change groups (*i.e.*, slow versus rapid progression).
Bede[8]	T1 at 0 and 4 months	100 ALS 100 controls	Decreased volume in pons and medulla at 4 month image; non-statistically significant reductions in brainstem volume over 4 months; vertex analysis showed medullary pyramid atrophy; decreased density in mesencephalic crura by morphometric analysis.
Cardenas-Blanco[9]	Longitudinal T1, DTI	34 ALS 29 controls	No DTI differences vs controls by multiple testing comparisons; lower FA and higher RD longitudinally; no cortical thickness, grey matter density, deep grey matter volume differences; FA does correlate with ALS progression.

Chipika[10]	MRI, T1 with Bayesian thalamus segmentation	100 ALS 117 controls	Atrophy of mediodorsal-paratenial-reuniens group of nuclei; In *C9orf72* negative ALS, decreased volume in motor nuclei, sensory nuclei, intralaminar, anteroventral, medial geniculate, and lateroposterior nuclei; decreased mediodorsal-paratenial-reuniens volumes in *C9orf72* positive ALS vs negative, but not statistically significant; vertex and morphometric analysis showed thalamic atrophy, but with some asymmetry
Contarino[11]	MRI, T1, spoiled gradient-echo T2, QSM	42 ALS 23 controls	Lower precentral cortical thickness; higher precentral susceptibility skewness.
Fabes[12]	Quantitative FLAIR intensity	33 ALS 21 controls	Higher FLAIR intensity in CST and corpus callosum.
Ferraro[13]	DTI	123 ALS 78 controls	Precentral cortical thickness differentiates ALS versus controls with 0.86 accuracy; DTI differentiates ALS versus controls with 0.78 accuracy; combined cortical thickness and DTI differentiates ALS versus controls with 0.91 accuracy; multimodal MRI improves classification accuracy for individual MND patients.
Grapperon[14]	^{23}Na MRI	27 ALS 30 controls	Higher total ^{23}Na; higher ^{23}Na in precentral gyri, CST, corpus callosum.
Hubers[15]	DTI, DWS	27 ALS 21 controls	Lower FA in corpus callosum motor segment/rostrum, CST; no DWS differences.
Kalra[16]	Longitudinal DTI	66 ALS 43 controls	Lower FA in CST, corticopontine tract, corticorubral tract, corticostriatal tract; FA of CST and frontal lobes declines with ALS progression.
Muller[17]	DTI	101 ALS 92 controls	Lower FA in CST, corticopontine tract, corticorubral tract, corticostriatal pathway.
Muller[18]	DTI	23 ALS 23 controls	Lower FA in CST, corticopontine tract, corticorubral tract.
Muller[19]	DTI	50 ALS 50 controls	Lower whole brain FA, CST, corticopontine tract, corticorubral tract, corticostriatal pathway, proximal portion of perforant path.

Qiu[2]	T1, DTI, RS fMRI	60 ALS 60 controls	Left precentral gyrus atrophy; higher cerebellar volume in Crus II, VIIb, VIIIa subregions; lower FA in left CST, corpus callosum body; lower functional connectivity in postcentral gyrus, precentral gyrus, cerebellum anterior lobe.
Ratai[20]	[^{11}C]-PBR28 PET, MR diffusion, ^{1}H-MRS	40 ALS	Precentral gyri, brainstem (test regions) vs precuneus (control region); positive myo-inositol/creatine and negative N-acetylaspartate/creatine correlations with [^{11}C]-PBR28 in precentral gyrus; higher myo-inositol/creatine and lower N-acetylaspartate/creatine correlation with lower FA.
Sassani[21]	^{31}P-MRS	20 ALS 10 controls	Lower mitochondrial oxidative phosphorylation in brainstem.
Schuster[22]	T1, DTI	81 ALS 66 controls	85·7% sensitivity, 78·4% specificity to discriminate ALS from control using average grey matter density of left/right precentral gyrus, average FA and RD of left/right superior corona radiata, inferior corona radiata, internal capsule, cerebral peduncles mesencephalic crus, CST pontine segment, average diffusivity of genu, corpus callosum corpus/splenium.
Schuster[23]	T1, DTI	60 ALS 69 controls	Clinical data predict 18-month survival 66·67% accuracy, 62·50% sensitivity, 70·84% specificity; MRI predict 18-month survival 77·08% accuracy, 79·16% sensitivity, 75% specificity using DTI of superior/inferior corona radiata, anterior/posterior limbs of internal capsule, cerebral peduncles (mesencephalic crus), corpus callosum genu, body, splenium and precentral/paracentral gyrus cortical thickness; combined MRI and clinical data predict 18-month survival 79·17% accuracy, 75% sensitivity, 83·34% specificity.

Senda[24]	Longitudinal T1, T2, DTI	67 ALS 38 controls	Lower grey matter volume in ALS: slow progressing group in motor cortex precentral knob, caudate head, medial front gyrus, thalamus, cingulate gyrus, intermediate progressing group in frontotemporal lobes, rapid progressing group more widespread and severe versus other 2 groups; lower FA in corona radiata and internal capsule of pyramidal tracts, widespread involvement tied to ALS progression.
Tu[25]	T1, DWI	20 ALS 31 controls	Lower thalamic volume; higher thalamic apparent diffusion.
Weidman[26]	DTI, QSM	38 ALS 15 MND mimics	Lower FA in CST; higher MD and RD in CST; higher QSM in maximum motor cortex.
Welton[27]	T1, arterial spin labelling (blood flow), susceptibility-weighted angiography (iron deposition), multiband kurtosis imaging (tissue microstructure)	21 ALS 63 controls	Lower volume and higher iron levels in symptomatic hemisphere; higher iron levels in motor cortex; lower diffusion kurtosis.
"Connectome" search criterion			
Basaia[28]	T1, T2, FLAIR, DTI, RS fMRI	173 ALS 79 controls	Altered structural global networks; lower mean structural local efficiency in sensorimotor, basal ganglia, frontal networks; longer path length in basal ganglia, frontal, temporal networks; lower mean nodal strength in frontal/temporal regions; lower FA in sensorimotor networks in precentral/postcentral gyri, supplementary motor area, basal ganglia, medial/lateral prefrontal cortex connections; higher functional connectivity in precentral gyrus, middle/superior frontal gyri.

Buchanan[29]	Diffusion, T1	30 ALS 30 controls	Motor (bilateral precentral and paracentral), frontal (left superior frontal, left-posterior cingulate), subcortical (bilateral pallidum, left thalamus, left caudate) subnetwork impairment; lower FA in CSF and corpus callosum; lower FA in CST linked to ALS progression rate.
Geevasinga[3]	T1, RS fMRI, TMS	20 ALS 20 controls	Higher connectivity in right inferior frontal triangularis and inferior frontal operculum to left and right fusiform regions, left inferior frontal operculum and left pallidum to right superior parietal cortex, “right Heschl's gyrus to left putamen and pallidum, right superior parietal to left supramarginal region, right fusiform region to right paracentral lobule, right angular gyrus to left anterior cingulum and left caudate”; higher functional connectivity, implying loss of long-range connections; lower grey matter volume in frontal lobe regions, rolandic operculum, right inferior orbital frontal region, precentral gyrus, postcentral gyrus, extrafrontal regions; lower SICI negative link with precentral gyrus nodal degree.
Meier[30]	Longitudinal DTI	208 ALS 208 controls	Spatiotemporal spread of connectome disruption involving more brain regions based on network-based statistics.
Schulthess[31]	DTI, RS fMRI, longitudinal in participant subset	135 ALS 56 controls	Higher functional connectivity in the motor (M1), brainstem (midbrain), ventral attention (ventral striatum), default mode/hippocampal intrinsic connectivity (cingulate cortex) networks; network expansion in longitudinal studies; lower FA in CST, corticopontine tract, corticorubral tract, corticostriatal pathway, proximal portion of perforant pathway; higher functional connectivity linked to worsening ALSFRS-R.
Serra[32]	DTI, RS fMRI	39 ALS 15 controls	Lower connectivity between frontal and temporal cortex, frontal and parietal cortex, temporal and occipital cortex; higher connectivity in limbic and subcortical grey matter and cingulate cortex.

van der Burgh[33]	T1, DWI MRI	292 ALS 156 controls	*C9orf72* negative participants: cortical thinning in primary motor, frontal/temporal regions, atrophy in left accumbens nucleus, right thalamus, bilateral hippocampi, left amygdala; lower connectivity. *C9orf72* positive participants: cortical thinning, atrophy in accumbens nucleus, bilateral thalami, hippocampi, amygdala, caudate, putamen, pallidum; lower connectivity, especially in bilateral precentral/paracentral gyri, basal ganglia, temporal lobe; cortical thinning more extensive with longer ALS duration.
"PET" search criterion			
Alshikho[34]	Integrated [^{11}C]-PBR28 PET-MRI	53 ALS 21 controls	Higher [^{11}C]-PBR28 uptake and cortical thinning in precentral and paracentral gyri.
D'Hulst[35]	[^{18}F]-FDG PET	Belgian cohort: 175 ALS 20 controls Italian cohort: 195 ALS 40 controls	Consistent [^{18}F]-FDG PET patterns in ALS vs controls; Belgian cohort, hypometabolism in frontal and parietal cortex, hypermetabolism in temporal cortex, cerebellum, brainstem; Italian cohort, hypometabolism in frontal, motor, occipital cortex, hypermetabolism in temporal cortex, cerebellum, brainstem.
Van Weehaeghe[36]	[^{18}F]-FDG PET	ALS group 1: 105 ALS group 2: 70 ALS 20 controls	Hypometabolism in frontal cortex, premotor cortex, inferolateral part of the parietal cortex; hypermetabolism in occipital cortical pole, cerebellum, upper brain stem, medial temporal cortex.

AD, axial diffusivity; ALSFRS-R, ALS functional rating scale-revised; CST, corticospinal tract; DTI, diffusion tensor imaging; DWI, diffusion weighted imaging; DWS, diffusion weighted magnetic resonance spectroscopy; FA, fractional anisotropy; FDG, fluorodeoxyglucose; FLAIR, fluid-attenuated inversion recovery; FTD, frontotemporal dementia; MD, mean diffusivity; MND, motor neuron disease; MO, mode; MRS, magnetic resonance spectroscopy; PLS, primary lateral sclerosis; PUMN, predominantly upper motor neuron disease; QSM, quantitative susceptibility mapping, detects iron-related changes; RD, radial diffusivity; RS fMRI, resting state functional MRI; SICI, short-interval intracortical inhibition; TMS, transcranial magnetic stimulation.

References

1. Mazón M, Vázquez Costa JF, Ten-Esteve A, Martí-Bonmatí L. Imaging Biomarkers for the Diagnosis and Prognosis of Neurodegenerative Diseases. The Example of Amyotrophic Lateral Sclerosis. *Front Neurosci*. 2018;12:784. doi:10.3389/fnins.2018.00784
2. Qiu T, Zhang Y, Tang X, et al. Precentral degeneration and cerebellar compensation in amyotrophic lateral sclerosis: A multimodal MRI analysis. *Hum Brain Mapp*. Aug 15 2019;40(12):3464-3474. doi:10.1002/hbm.24609
3. Geevasinga N, Korgaonkar MS, Menon P, et al. Brain functional connectome abnormalities in amyotrophic lateral sclerosis are associated with disability and cortical hyperexcitability. *Eur J Neurol*. Dec 2017;24(12):1507-1517. doi:10.1111/ene.13461
4. Costagli M, Donatelli G, Biagi L, et al. Magnetic susceptibility in the deep layers of the primary motor cortex in Amyotrophic Lateral Sclerosis. *Neuroimage Clin*. 2016;12:965-969. doi:10.1016/j.nicl.2016.04.011
5. Acosta-Cabronero J, Machts J, Schreiber S, et al. Quantitative Susceptibility MRI to Detect Brain Iron in Amyotrophic Lateral Sclerosis. *Radiology*. Oct 2018;289(1):195-203. doi:10.1148/radiol.2018180112
6. Alruwaili AR, Pannek K, Coulthard A, Henderson R, Kurniawan ND, McCombe P. A combined tract-based spatial statistics and voxel-based morphometry study of the first MRI scan after diagnosis of amyotrophic lateral sclerosis with subgroup analysis. *J Neuroradiol*. Feb 2018;45(1):41-48. doi:10.1016/j.neurad.2017.03.007
7. Baek SH, Park J, Kim YH, et al. Usefulness of diffusion tensor imaging findings as biomarkers for amyotrophic lateral sclerosis. *Sci Rep*. Mar 23 2020;10(1):5199. doi:10.1038/s41598-020-62049-0
8. Bede P, Chipika RH, Finegan E, et al. Brainstem pathology in amyotrophic lateral sclerosis and primary lateral sclerosis: A longitudinal neuroimaging study. *Neuroimage Clin*. 2019;24:102054. doi:10.1016/j.nicl.2019.102054
9. Cardenas-Blanco A, Machts J, Acosta-Cabronero J, et al. Structural and diffusion imaging versus clinical assessment to monitor amyotrophic lateral sclerosis. *NeuroImage: Clinical*. 2016/01/01/ 2016;11:408-414. doi:https://doi.org/10.1016/j.nicl.2016.03.011
10. Chipika RH, Finegan E, Li Hi Shing S, et al. "Switchboard" malfunction in motor neuron diseases: Selective pathology of thalamic nuclei in amyotrophic lateral sclerosis and primary lateral sclerosis. *Neuroimage Clin*. 2020;27:102300. doi:10.1016/j.nicl.2020.102300
11. Contarino VE, Conte G, Morelli C, et al. Toward a marker of upper motor neuron impairment in amyotrophic lateral sclerosis: A fully automatic investigation of the magnetic susceptibility in the precentral cortex. *Eur J Radiol*. Mar 2020;124:108815. doi:10.1016/j.ejrad.2020.108815
12. Fabes J, Matthews L, Filippini N, Talbot K, Jenkinson M, Turner MR. Quantitative FLAIR MRI in Amyotrophic Lateral Sclerosis. *Acad Radiol*. Oct 2017;24(10):1187-1194. doi:10.1016/j.acra.2017.04.008
13. Ferraro PM, Agosta F, Riva N, et al. Multimodal structural MRI in the diagnosis of motor neuron diseases. *Neuroimage Clin*. 2017;16:240-247. doi:10.1016/j.nicl.2017.08.002
14. Grapperon AM, Ridley B, Verschueren A, et al. Quantitative Brain Sodium MRI Depicts Corticospinal Impairment in Amyotrophic Lateral Sclerosis. *Radiology*. Aug 2019;292(2):422-428. doi:10.1148/radiol.2019182276

15. Hubers A, Bockler B, Abaei A, et al. Functional and structural impairment of transcallosal motor fibres in ALS: a study using transcranial magnetic stimulation, diffusion tensor imaging, and diffusion weighted spectroscopy. *Brain Imaging Behav*. Apr 2021;15(2):748-757. doi:10.1007/s11682-020-00282-x

16. Kalra S, Müller HP, Ishaque A, et al. A prospective harmonized multicenter DTI study of cerebral white matter degeneration in ALS. *Neurology*. Aug 25 2020;95(8):e943-e952. doi:10.1212/wnl.0000000000010235

17. Muller HP, Agosta F, Riva N, et al. Fast progressive lower motor neuron disease is an ALS variant: A two-centre tract of interest-based MRI data analysis. *Neuroimage Clin*. 2018;17:145-152. doi:10.1016/j.nicl.2017.10.008

18. Muller HP, Gorges M, Del Tredici K, Ludolph AC, Kassubek J. The same cortico-efferent tract involvement in progressive bulbar palsy and in 'classical' ALS: A tract of interest-based MRI study. *Neuroimage Clin*. 2019;24:101979. doi:10.1016/j.nicl.2019.101979

19. Muller HP, Gorges M, Kassubek R, Dorst J, Ludolph AC, Kassubek J. Identical patterns of cortico-efferent tract involvement in primary lateral sclerosis and amyotrophic lateral sclerosis: A tract of interest-based MRI study. *Neuroimage Clin*. 2018;18:762-769. doi:10.1016/j.nicl.2018.03.018

20. Ratai EM, Alshikho MJ, Zurcher NR, et al. Integrated imaging of [(11)C]-PBR28 PET, MR diffusion and magnetic resonance spectroscopy (1)H-MRS in amyotrophic lateral sclerosis. *Neuroimage Clin*. 2018;20:357-364. doi:10.1016/j.nicl.2018.08.007

21. Sassani M, Alix JJ, McDermott CJ, et al. Magnetic resonance spectroscopy reveals mitochondrial dysfunction in amyotrophic lateral sclerosis. *Brain*. Dec 1 2020;143(12):3603-3618. doi:10.1093/brain/awaa340

22. Schuster C, Hardiman O, Bede P. Development of an Automated MRI-Based Diagnostic Protocol for Amyotrophic Lateral Sclerosis Using Disease-Specific Pathognomonic Features: A Quantitative Disease-State Classification Study. *PLoS One*. 2016;11(12):e0167331. doi:10.1371/journal.pone.0167331

23. Schuster C, Hardiman O, Bede P. Survival prediction in Amyotrophic lateral sclerosis based on MRI measures and clinical characteristics. *BMC Neurol*. Apr 17 2017;17(1):73. doi:10.1186/s12883-017-0854-x

24. Senda J, Atsuta N, Watanabe H, et al. Structural MRI correlates of amyotrophic lateral sclerosis progression. *J Neurol Neurosurg Psychiatry*. Nov 2017;88(11):901-907. doi:10.1136/jnnp-2016-314337

25. Tu S, Menke RAL, Talbot K, Kiernan MC, Turner MR. Regional thalamic MRI as a marker of widespread cortical pathology and progressive frontotemporal involvement in amyotrophic lateral sclerosis. *J Neurol Neurosurg Psychiatry*. Dec 2018;89(12):1250-1258. doi:10.1136/jnnp-2018-318625

26. Weidman EK, Schweitzer AD, Niogi SN, et al. Diffusion tensor imaging and quantitative susceptibility mapping as diagnostic tools for motor neuron disorders. *Clin Imaging*. Jan - Feb 2019;53:6-11. doi:10.1016/j.clinimag.2018.09.015

27. Welton T, Maller JJ, Lebel RM, Tan ET, Rowe DB, Grieve SM. Diffusion kurtosis and quantitative susceptibility mapping MRI are sensitive to structural abnormalities in amyotrophic lateral sclerosis. *Neuroimage Clin*. 2019;24:101953. doi:10.1016/j.nicl.2019.101953

28. Basaia S, Agosta F, Cividini C, et al. Structural and functional brain connectome in motor neuron diseases: A multicenter MRI study. *Neurology*. Nov 3 2020;95(18):e2552-e2564. doi:10.1212/WNL.0000000000010731

29. Buchanan CR, Pettit LD, Storkey AJ, Abrahams S, Bastin ME. Reduced structural connectivity within a prefrontal-motor-subcortical network in amyotrophic lateral sclerosis. *J Magn Reson Imaging*. May 2015;41(5):1342-52. doi:10.1002/jmri.24695

30. Meier JM, van der Burgh HK, Nitert AD, et al. Connectome-Based Propagation Model in Amyotrophic Lateral Sclerosis. *Ann Neurol*. May 2020;87(5):725-738. doi:10.1002/ana.25706

31. Schulthess I, Gorges M, Muller HP, et al. Functional connectivity changes resemble patterns of pTDP-43 pathology in amyotrophic lateral sclerosis. *Sci Rep*. Dec 8 2016;6:38391. doi:10.1038/srep38391

32. Serra A, Galdi P, Pesce E, et al. Strong-Weak Pruning for Brain Network Identification in Connectome-Wide Neuroimaging: Application to Amyotrophic Lateral Sclerosis Disease Stage Characterization. *Int J Neural Syst*. Sep 2019;29(7):1950007. doi:10.1142/S0129065719500072

33. van der Burgh HK, Westeneng HJ, Walhout R, et al. Multimodal longitudinal study of structural brain involvement in amyotrophic lateral sclerosis. *Neurology*. Jun 16 2020;94(24):e2592-e2604. doi:10.1212/wnl.0000000000009498

34. Alshikho MJ, Zurcher NR, Loggia ML, et al. Integrated magnetic resonance imaging and [(11) C]-PBR28 positron emission tomographic imaging in amyotrophic lateral sclerosis. *Ann Neurol*. Jun 2018;83(6):1186-1197. doi:10.1002/ana.25251

35. D'Hulst L, Van Weehaeghe D, Chio A, et al. Multicenter validation of [(18)F]-FDG PET and support-vector machine discriminant analysis in automatically classifying patients with amyotrophic lateral sclerosis versus controls. *Amyotroph Lateral Scler Frontotemporal Degener*. Nov 2018;19(7-8):570-577. doi:10.1080/21678421.2018.1476548

36. Van Weehaeghe D, Ceccarini J, Delva A, Robberecht W, Van Damme P, Van Laere K. Prospective Validation of 18F-FDG Brain PET Discriminant Analysis Methods in the Diagnosis of Amyotrophic Lateral Sclerosis. *J Nucl Med*. Aug 2016;57(8):1238-43. doi:10.2967/jnumed.115.166272